Journal of Materials Chemistry A

PAPER

View Article Online
View Journal | View Issue

Cite this: J. Mater. Chem. A, 2014, 2, 12924

Redox-crosslinked graphene networks with enhanced electrochemical capacitance†

Wei Ai,[a] Xiehong Cao,[c] Zhipeng Sun,[a] Jian Jiang,[a] Zhuzhu Du,[b] Linghai Xie,[b] Yanlong Wang,[a] Xingjue Wang,[a] Hua Zhang,[c] Wei Huang*[be] and Ting Yu*[ad]

Received 17th March 2014
Accepted 9th June 2014

DOI: 10.1039/c4ta01309c

www.rsc.org/MaterialsA

A facile and effective method for the synthesis of redox-crosslinked graphene networks is reported. This method involves the polyphosphoric acid-catalyzed cyclization reaction between the carboxylic groups on graphene oxide and the hydroxyl, amino groups on 4,6-diaminoresorcinol hydrochloride, as well as a subsequent reduction process. The obtained benzobisoxazole-crosslinked graphene networks (BBO-GNs) show a high BET surface area of 357 $m^2 g^{-1}$ in comparison with the reduced graphene oxide (rGO) (117 $m^2 g^{-1}$), due to the presence of benzobisoxazole groups that prevent the irreversible restacking or agglomeration of graphene sheets during the reduction. Another immediate and more practically meaningful benefit of introducing benzobisoxazole groups is that such functional groups could effectively provide an extra contributing channel to the specific capacity by pseudocapacitance. As a consequence, the improved performance such as significantly enhanced electrochemical capacitance is clearly demonstrated in the supercapacitor with the electrodes of BBO-GNs.

1. Introduction

With the rapid depletion of finite fossil fuels and global pollution caused by their consumption, the increase of environmental awareness in modern society requires the development of clean, green and renewable energy sources that can substitute traditional fossil fuels for a sustainable world.[1] Therefore, novel energy conversion and storage technologies of high performance are needed to satisfy the increasing demand for energy.[2] In this regard, lithium-ion batteries (LIBs) and supercapacitors have attracted a great deal of attention due to their high energy storage capability.[3,4] As hybrid power sources for electrical vehicles, supercapacitors are more promising than LIBs owing to their high power density, fast charging/discharging rates and wide operating temperature range, as well as excellent safety.[5] Based on the charge storage mechanism, supercapacitors are mainly classified into electrochemical double layer capacitors (EDLCs) and pseudocapacitors.[6,7] EDLCs store energy by accumulated charge at the electrode/electrolyte interface through a non-faradic process, whereas pseudocapacitors store energy somehow like LIBs by reversible faradic redox reactions at or near the electrode surface. It is generally believed that pseudocapacitors can exhibit about 10–100 times higher specific capacitance than EDLCs.[8] However, pseudocapacitors usually suffer from unsatisfactory cycling stability and rate performance since the conductivity of electrode materials (redox-active polymers or transition metal oxides) cannot support fast electron transport at high rates, which seriously hindered their practical applications.[9] In contrast to pseudocapacitors, EDLCs can exhibit longer cycling stability and higher power density.

Current commercial EDLCs rely on the use of carbon-based electrode materials owing to their high surface areas for ion adsorption, high conductivity, low cost and relative ease of preparation.[10] Graphene, a one-atom-thick sheet of sp^2-bonded carbon atoms arranged in a honeycomb lattice, has been intensively studied as the electrode material for supercapacitors since its first preparation in 2004, because of its fascinating structure and excellent physical properties together with the natural abundance of its precursor, graphite.[11,12] The specific capacitance of graphene can reach 550 F g^{-1} if the theoretical specific surface area (2630 $m^2 g^{-1}$) could be fully utilized for EDLCs.[13] Nevertheless, direct synthesis of high-quality

[a]Division of Physics and Applied Physics, School of Physical and Mathematical Sciences, Nanyang Technological University, 637371, Singapore. E-mail: yuting@ntu.edu.sg; Fax: +65 63167899; Tel: +65 63167899

[b]Key Laboratory for Organic Electronics & Information Displays (KLOEID) and Institute of Advanced Materials (IAM), Nanjing University of Posts and Telecommunications, 9 Wenyuan Road, Nanjing 210023, China. E-mail: wei-huang@njupt.edu.cn; Fax: +86 25 83492333; Tel: +86 25 83492333

[c]School of Materials Science and Engineering, Nanyang Technological University, 639798, Singapore

[d]Graphene Research Centre, National University of Singapore, 117546, Singapore

[e]Jiangsu-Singapore Joint Research Center for Organic/Bio-Electronics & Information Displays and Institute of Advanced Materials, Nanjing Tech University, Nanjing 211816, China

† Electronic supplementary information (ESI) available: The C 1s XPS spectra of GO, rGO and BBO-GNs. TGA curves, N_2 adsorption–desorption isotherms, pore size distributions and EIS of rGO and BBO-GNs. The proposed electrochemical reactions on BBO-GNs. CV curves of the graphite electrode, rGO and BBO-GN samples. See DOI: 10.1039/c4ta01309c

graphene for supercapacitors suffers from high cost that significantly limits its large scale application.[14] On the other hand, chemical oxidation and exfoliation of graphite into graphene oxide (GO), followed by reduction, allow the mass production of graphene at low cost. However, graphene sheets tend to form irreversible agglomerates or even restack to graphite through strong π–π stacking and van der Waals interaction during the reduction, resulting in severe loss of the surface area for supercapacitor applications.[15,16] In our previous study, we synthesized heterocyclic grafted graphene, which showed good electrochemical performance as the electrode material for supercapacitors owing to the effectiveness of functionalization in preventing the restacking of graphene sheets.[17] Besides this, the introduction of redox-active functional groups into graphene has also been regarded as an effective strategy to further improve the electrochemical capacitance of graphene by providing additional redox capacitance.[18] Therefore, supercapacitors of high performance require that the electrode materials possess not only high surface area for electric double-layer capacitance but also combine with redox-active species for pseudocapacitance.

Herein, we report a facile and effective method for the synthesis of benzobisoxazole-crosslinked graphene networks (BBO-GNs) through a polyphosphoric acid-catalyzed cyclization reaction between the carboxylic groups on GO and the hydroxyl and amino groups on 4,6-diaminoresorcinol hydrochloride (DAR·2HCl) followed by a reduction process. Benefiting from the introduced benzobisoxazole groups, restacking of the graphene sheets during the reduction process is effectively prevented. Thus, the BBO-GNs exhibit enhanced electrochemical capacitance compared with that of rGO. This is attributed to the synergistic effect of the high surface area of BBO-GNs that leads to large charge storage and the redox-active benzobisoxazole groups that provide additional pseudocapacitance from fast and reversible faradic reactions.

2. Experimental section

2.1 Materials

All chemicals were purchased from Sigma-Aldrich and used without further purification.

2.2 Synthesis of graphite oxide

Graphite oxide was synthesized from graphite according to a modified Hummers' method. The details are described in the literature.[19]

2.3 Synthesis of BBO-GNs

The synthesis of BBO-GNs is schematically shown in Scheme 1.[20] Briefly, 200 mg graphite oxide was dispersed in 100 mL deionized water by sonication for 50 min, followed by 10 min centrifugation at 1000 rpm to remove the unexfoliated particles. Then, 159.8 mg DAR·2HCl was added, and the mixture was sonicated for another 5 min. After that, 1.25 mL polyphosphoric acid (PPA) was dropwise added under vigorous stirring. The solution was refluxed at 80 °C in the dark for 24 h, and purified

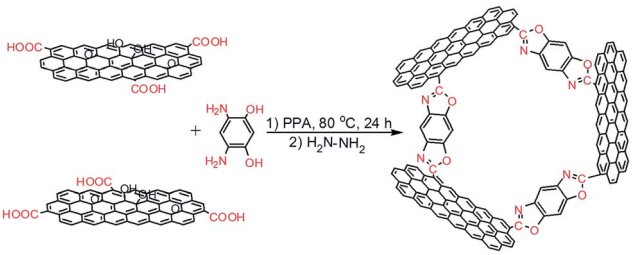

Scheme 1 Synthetic procedure for BBO-GNs.

by filtration and washing (1 : 2 HCl and then water, 4 times each). The as-obtained product was redispersed into 100 mL deionized water by sonication, and then 1.4 mL hydrazine hydrate was added and refluxed at 80 °C for 24 h. Finally, the product was filtered and washed with deionized water several times, and then dried under vacuum conditions.

2.4 Synthesis of rGO

rGO was synthesized *via* chemical reduction of exfoliated GO by hydrazine. Typically, 100 mL GO solution (2 mg mL^{-1}) was prepared by ultrasonic exfoliation of graphite oxide in deionized water and centrifuged at 1000 rpm for 10 min to remove the unexfoliated particles. Then, 1.4 mL hydrazine hydrate was added and the mixture was kept at 80 °C for 24 h. The product was collected by filtration, washed with deionized water several times, and dried under vacuum conditions.

2.5 Characterization

Fourier-transform infrared spectra (FT-IR) were recorded using the KBr-pellet method in transmission mode on a NEXUS 670 FT-IR spectrometer. X-ray photoelectron spectroscopy (XPS) analysis was performed on an ESCALAB MK II X-ray photoelectron spectrometer using an Al Kα (1486.6 eV) X-ray source. Field-emission scanning electron microscopy (FESEM) analysis was conducted with a JEOL JSM-6700F electron microscope with an accelerating voltage of 10 kV. Transmission electron microscopy (TEM) measurements were conducted on a JEOL JEM-2010 transmission electron microscope with an accelerating voltage of 200 kV. Raman spectra were collected using a WITEC CRM200 Raman system with a 532 nm excitation laser. The surface area was measured by nitrogen adsorption–desorption isotherms using the Brunauer–Emmett–Teller (BET) method on a Micromeritics ASAP 2020. Thermogravimetric analysis (TGA) was conducted using a Shimadzu DTG-60H at a heating rate of 5 °C min^{-1} from room temperature to 800 °C under nitrogen flow.

2.6 Electrochemical measurements

The electrochemical measurements were performed on a CHI 760D electrochemical workstation using a three-electrode cell system in a 1 mol L^{-1} H_2SO_4 aqueous electrolyte. The working electrodes were prepared by mixing the active materials (80 wt%), acetylene black (10 wt%) and polyvinylidene fluoride (PVDF, 10 wt%) in *N*-methyl-2-pyrrolidone (NMP). After that, the

mixture was coated onto the graphite paper (1 cm × 2 cm) as the working electrode, which was then dried in a vacuum at 100 °C for 12 h to remove the solvent.[21] Platinum foil (1 cm × 1 cm) and a saturated calomel electrode (SCE) were used as the counter and reference electrodes, respectively. The potential window for electrochemical measurements was confined between −0.3 and 0.7 V. Electrochemical impedance spectroscopy (EIS) measurements were carried out in the frequency range from 100 kHz to 0.1 Hz at 5 mV amplitude. The specific capacitances were calculated using the equation $C = Q/2mV$ from the CV curves, where Q is half the integrated area of the cyclic voltammetry (CV) curve, m is the mass of the active material, and V is the width of the potential window. While the specific capacitances derived from galvanostatic discharge curves were calculated based on the following equation: $C = I\Delta t/m\Delta V$, where I is the discharge current, Δt is the discharge time, m is the mass of the active material, and ΔV represents the potential window.

3. Results and discussion

3.1 Materials characterization

The successful functionalization of graphene with benzobisoxazole groups was confirmed by FT-IR spectra and XPS measurements. Fig. 1A shows the FT-IR spectra of the samples. In the FT-IR spectrum of GO, the characteristic peaks at ~1727, ~1225 and 1053 cm^{-1} are attributed to the C=O stretching, C–OH stretching and C–O stretching modes, respectively.[22,23] The peak at ~1630 cm^{-1} is assigned to the O–H deformation mode of the adsorbed water molecules.[24] As expected, the peaks belonging to the oxygen-containing functional groups either disappeared or their intensities significantly decreased in the FT-IR spectra of rGO and BBO-GNs, which suggests the reduction of GO. While for BBO-GNs, additional peaks at ~1561 and 1438 cm^{-1} were observed corresponding to the stretching mode of C=N and C–N, respectively, indicating that graphene has been functionalized with benzobisoxazole groups.[25,26] The C 1s XPS spectrum of GO (Fig. S1A†) suggests the presence of four components: C–C (284.6 eV), C–O (286.7 eV), C=O (288.0 eV), and O–C=O (289.1 eV). Obviously, the peak intensities of the oxygen-containing functional groups are dramatically decreased in the spectra of rGO and BBO-GNs (Fig. S1B and C†), which further confirms the reduction of GO. Moreover, the appearance of the C–N peak at 285.6 eV in the C 1s XPS spectrum of BBO-GNs indicates the introduction of N functionalities into graphene sheets. High-resolution N 1s XPS spectrum (Fig. 1B) analysis of BBO-GNs shows a single peak at 399.5 eV, corresponding to the pyridine-like N. The above results clearly indicate that benzobisoxazole groups have been successfully introduced into the graphene sheets.

Raman spectroscopy was also used to investigate the structural changes of the materials after the functionalization and reduction. As shown in Fig. 1C, the Raman spectrum of GO shows two remarkable peaks centered at 1354 and 1600 cm^{-1}, corresponding to the breathing mode of the k-point phonons of A_{1g} symmetry (D band) and in-plane vibrations of sp^2-bonded carbon atoms (G band), respectively.[27] The G band of rGO is blue-shifted to 1588 cm^{-1} due to the removal of the oxygen-containing functional groups. It is noted that the frequencies of the D and G bands in the BBO-GNs are very similar to that observed in GO, which implies that the skeleton structure of graphene sheets has been maintained in BBO-GNs.[28] Generally, the I_D/I_G ratio is used to measure the degree of disorder and impurities in graphene-based materials.[29] In comparison to GO, the increased I_D/I_G ratio of BBO-GNs could be due to the functionalization induced defects and disordered crystal structure of the graphene sheets.[30] rGO exhibits a higher I_D/I_G value (1.09) compared to those of GO (0.99) and BBO-GNs (1.03), which might result from the formation of numerous small sp^2 domains in graphene sheets after reduction.[31] Moreover, the

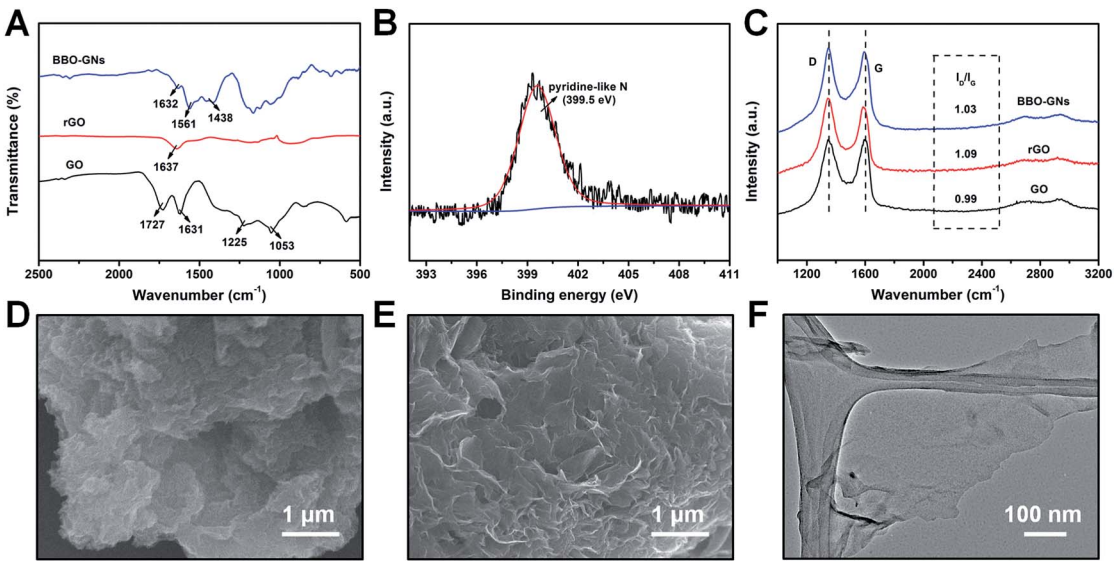

Fig. 1 (A) FT-IR spectra of GO, rGO and BBO-GNs. (B) N 1s XPS spectra of BBO-GNs. (C) Raman spectra of GO, rGO and BBO-GNs. FESEM images of rGO (D) and BBO-GNs (E). (F) TEM image of BBO-GNs.

Raman bands of oxazole heterocycles are not observed in the Raman spectrum of BBO-GNs due to their relatively low content (~20%) as shown in the TGA results (Fig. S2†).[32]

The morphologies of rGO and BBO-GNs were characterized by FESEM and TEM as shown in Fig. 1D–F. rGO shows a stacked graphite-like structure (Fig. 1D) arising from the face-to-face aggregation of the graphene sheets during the reduction process, whereas BBO-GNs exhibit a scaly-like structure (Fig. 1E) due to the chemical cross-linking of graphene sheets by the benzobisoxazole groups. Moreover, the TEM image (Fig. 1F) reveals that the layer-like structure with intrinsic wrinkle folding feature was observed in BBO-GNs, indicating that the introduced benzobisoxazole groups can prevent the restacking of the graphene sheets to some extent.[23,33]

To further examine the porous structure of the samples, nitrogen adsorption–desorption isotherms and the corresponding Barrett–Joyner–Halenda (BJH) pore size distributions were measured (Fig. 2 and S3†). Both rGO and BBO-GNs exhibit the isotherms close to type IV, which belongs to the mesoporous structures.[34] The BET surface area of rGO (117 $m^2 g^{-1}$) is much smaller than the theoretical specific surface area of graphene (2630 $m^2 g^{-1}$) due to the severe restacking of graphene sheets during reduction.[35] However, the BET surface area of BBO-GNs could reach as high as 357 $m^2 g^{-1}$, three times that of rGO, once again demonstrating that the introduced benzobisoxazole groups can prevent the restacking of graphene sheets.[36] Although this value is not as high as those of the previous reports, BBO-GNs still exhibit high supercapacitor performance due to their unique structure (see the discussion below).[37] Pore size distribution curves (Fig. 2B and S3B†) confirmed that rGO and BBO-GNs possess a multiple pore structure (micropores, mesopores and macropores) due to the overlapping or cross-linking of the graphene sheets.[18] Additionally, BBO-GNs have a larger pore volume (0.22 $cm^3 g^{-1}$) than that of rGO (0.14 $cm^3 g^{-1}$),

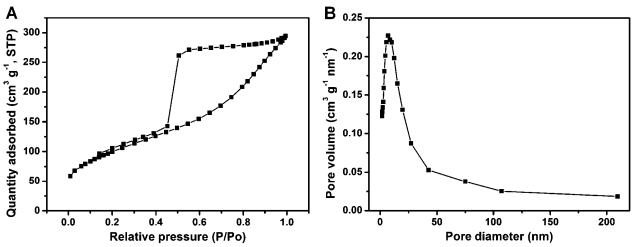

Fig. 2 N_2 adsorption–desorption isotherms (A) and pore size distributions (B) of BBO-GNs.

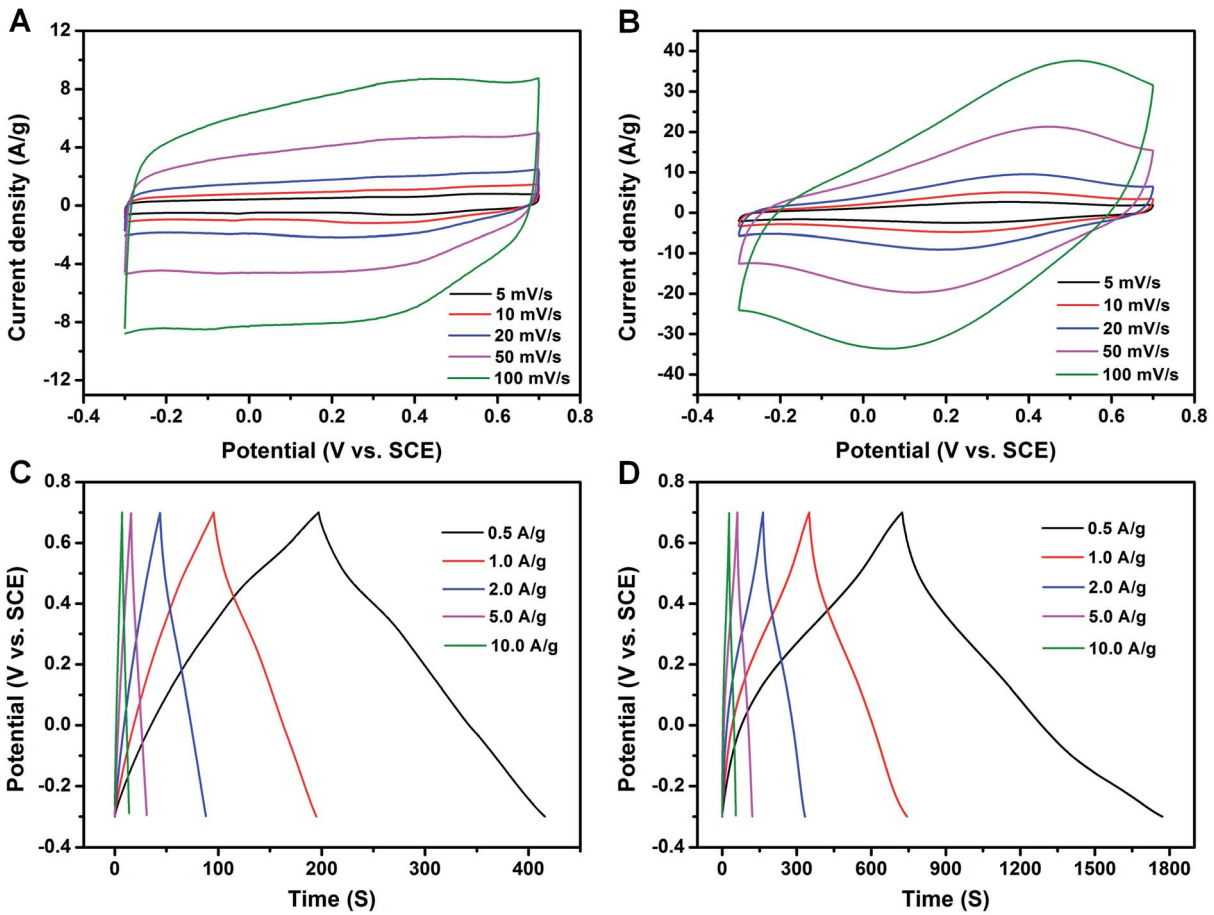

Fig. 3 CV curves of the rGO (A) and BBO-GNs (B) samples at different scan rates. Charge–discharge curves of rGO (C) and BBO-GNs (D) samples at various current densities.

which is favorable for the transportation and diffusion of electrolyte ions during the fast charge–discharge process.[38]

3.2 Electrochemical measurements

To evaluate the electrochemical properties of rGO and BBO-GNs as supercapacitor electrodes, a three-electrode system was constructed in 1 M H_2SO_4 aqueous electrolyte with a potential range from −0.3 to 0.7 V (*vs.* SCE). The higher current density of BBO-GNs suggests their superior electrochemical performance to rGO (Fig. S4†). Fig. 3A and B show the CV curves of rGO and BBO-GNs at different scan rates. Evidently, rGO exhibits typical rectangular CV curves at scan rates of 5–100 mV s^{-1}, implying an ideal electric double-layer capacitance behavior.[39] While BBO-GNs display a pair of redox peaks in the potential range of −0.1 to 0.5 V, which corresponds to the reversible redox reaction of the covalently grafted benzobisoxazole groups (Scheme S1†),[17] indicating the presence of both electric double-layer capacitance and pseudocapacitance. Meanwhile, when the scan rate increases from 5 to 100 mV s^{-1}, the CV curves of BBO-GNs basically maintain the redox peak-incorporated rectangular shape, which implies a quick charge-propagation capability in the BBO-GN electrode. Fig. 4 shows the capacitance values of rGO and BBO-GNs calculated from CV curves. It is clear that BBO-GN electrodes exhibit a much larger capacitance than the rGO electrode. Specifically, at a scan rate of 5 mV s^{-1}, the specific capacitance of BBO-GNs is 345.6 F g^{-1}, which is more than three times higher than that of rGO (99.4 F g^{-1}) and also higher than the previously reported graphene-based materials.[40,41] The decrease of the specific capacitance with increasing scan rate is due to the diffusion limit of electrolyte ions into the electrode materials.

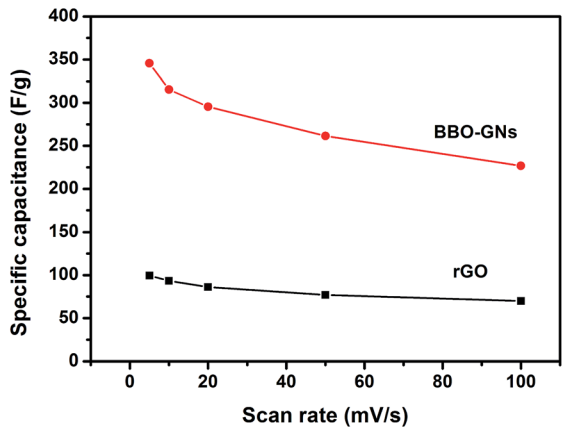

Fig. 4 Specific capacitance as a function of scan rate for rGO and BBO-GN samples.

Galvanostatic charge–discharge measurements were performed at various current densities to further investigate the electrochemical performances of the rGO and BBO-GN electrodes. As shown in Fig. 3C and D, the discharge time of BBO-GNs is significantly longer than that of rGO at the same discharging rate, indicating that BBO-GNs have a much larger capacitance. Moreover, the charge–discharge curves of BBO-GNs show a deviation from linearity due to the contribution of pseudocapacitance, which is in agreement with CV results. The BBO-GN electrode shows a large specific capacitance of 523.5 F g^{-1} at a current density of 0.5 A g^{-1}, which is nearly five times that of the rGO electrode (109.5 F g^{-1}). When the current density increases from 0.5 to 10 A g^{-1}, the specific capacitances of rGO and BBO-GNs vary from 109.5 to 68 F g^{-1} and 523.5 to 270 F g^{-1}, respectively. It is noteworthy that even at a current density of 10 A g^{-1}, the specific capacitance of BBO-GNs remains at 270 F g^{-1}, which is ~70% of that at 1 A g^{-1} and still 3.97 times higher than that of rGO (68 F g^{-1}), indicating a good rate capability of BBO-GNs. The above results indicate that the introduced benzobisoxazole groups played an essential role in the high specific capacitance of BBO-GNs.

The cycling stability test over 9000 cycles for the BBO-GN electrode was carried out at a scan rate of 1 V s^{-1}, as shown in

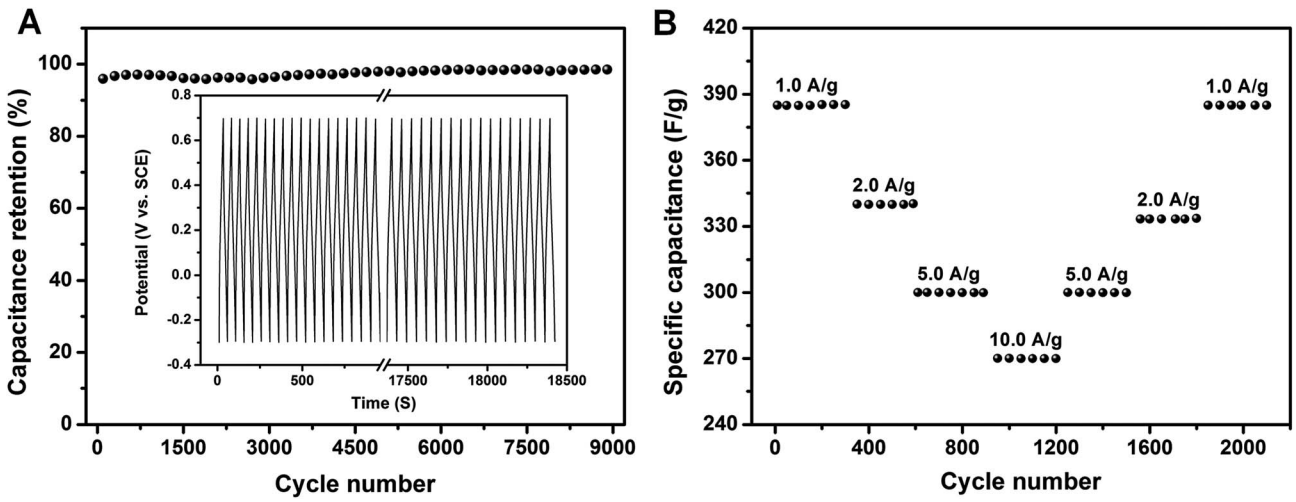

Fig. 5 (A) Cycling stability of the BBO-GN sample at a scan rate of 1 V s^{-1}. The inset shows the charge–discharge curves for the first 300 cycles at 10 A g^{-1}. (B) Cycling performance of the BBO-GN sample at various current densities.

Fig. 5A. The increase of specific capacitance during the first 300 cycles may arise from the activation process, which results in the enhanced contacting area of the electrode material with the electrolyte.[42,43] It is clear that the BBO-GN electrode exhibits an excellent electrochemical stability, indicating that the introduced benzobisoxazole groups are highly stable to sustain a long-term cycling stability. To highlight the superior electrochemical performance of the BBO-GN electrode, the cycling performance was further evaluated at a stepwise current density increasing from 1 to 10 A g^{-1} (Fig. 5B). Notably, the BBO-GN electrode still exhibits the stable specific capacitance at each current density, even when suffering from a sudden change of the current delivery. Furthermore, on switching the current density back to 1 A g^{-1}, the specific capacitance of the BBO-GN electrode is able to recover to the initial value, implying its excellent reversibility. These results demonstrate that BBO-GNs are a high performance supercapacitor electrode material with both long-term cycling stability and excellent rate capability. EIS was also employed to investigate the rGO and BBO-GN electrodes. As shown in Fig. S5,† the equivalent series resistance (ESR) of the BBO-GN electrode (1.6 Ω) is much smaller than that of the rGO electrode (15.5 Ω), indicating a lower charge-transfer resistance.[44]

The improved electrochemical performance of the BBO-GNs is attributed to their unique features of composition and structure. The covalently grafted benzobisoxazole groups prevented the restacking of the graphene sheets, which gives a large BET surface area of BBO-GNs for easy access to the electrolyte and also shortens the ion diffusion length. On the other hand, the introduced benzobisoxazole groups greatly enhanced the specific capacitance of graphene due to the contribution of additional pseudocapacitance. Besides, the crosslinked graphene networks can promote rapid electron transport for the faradic reactions, whereas the as-formed mesoporous structure can facilitate the ion diffusion through the electrode.

4. Conclusions

In summary, we have developed an efficient strategy to fabricate redox-crosslinked graphene networks *via* chemical engineering of graphene. The large surface area and additional pseudocapacitance make BBO-GNs a high performance electrode material for supercapacitors in terms of high specific capacitance (393.6 F g^{-1} at a current density of 1.0 A g^{-1}) and excellent cycling stability (9000 cycles with 98.4% retention), which are superior to the previously reported graphene-based materials.[40,41] Our results demonstrate that the covalent functionalization of graphene with redox-active species can greatly enhance its supercapacitive performance due to the combinational effects of electric double-layer capacitance and pseudocapacitance. The method developed in this work may open up a new route to further improve the electrochemical performance of graphene for electrochemical energy storage applications.

Acknowledgements

This work is supported by the Singapore National Research Foundation under NRF RF Award no. NRFRF2010-07, A*Star SERC PSF grant 1321202101 and MOE Tier 2 MOE2012-T2-2-049. H.Z. thanks the support from Singapore MOE under AcRF Tier 2 (ARC 26/13, no. MOE2013-T2-1-034) and AcRF Tier 1 (RG 61/12), and the Start-Up Grant (M4080865.070.706022) in NTU. This research is also funded by the Singapore National Research Foundation and the publication is supported under the Campus for Research Excellence and Technological Enterprise (CREATE) programme (Nanomaterials for Energy and Water Management). The authors thank the help of Mr Taixing Tan (Key Laboratory of Functional Inorganic Material Chemistry, Heilongjiang University) for the BET and TGA characterizations.

Notes and references

1 M. A. Sutton and A. Bleeker, *Nature*, 2013, **494**, 435.
2 K. G. Reddy, T. G. Deepak, G. S. Anjusree, S. Thomas, S. Vadukumpully, K. R. V. Subramanian, S. V. Nair and A. S. Nair, *Phys. Chem. Chem. Phys.*, 2014, **16**, 6838.
3 W. Ai, Z. Du, Z. Fan, J. Jiang, Y. Wang, H. Zhang, L. Xie, W. Huang and T. Yu, *Carbon*, 2014, **76**, 148.
4 Z. Cui, W. Yuan and C. M. Li, *J. Mater. Chem. A*, 2013, **1**, 12926.
5 C. X. Guo and C. M. Li, *Energy Environ. Sci.*, 2011, **4**, 4504.
6 P. Simon and Y. Gogotsi, *Nat. Mater.*, 2008, **7**, 845.
7 L. Sun, Y. Fu, C. Tian, Y. Yang, L. Wang, J. Yin, J. Ma, R. Wang and H. Fu, *ChemSusChem*, 2014, **7**, 1637, DOI: 10.1002/cssc.201400048.
8 B. E. Conway, V. Birss and J. Wojtowicz, *J. Power Sources*, 1997, **66**, 1.
9 Z. Cui, C. X. Guo, W. Yuan and C. M. Li, *Phys. Chem. Chem. Phys.*, 2012, **14**, 12823.
10 E. Frackowiak, *Phys. Chem. Chem. Phys.*, 2007, **9**, 1774.
11 S. Han, D. Wu, S. Li, F. Zhang and X. Feng, *Adv. Mater.*, 2014, **26**, 849.
12 L. Jiang and Z. Fan, *Nanoscale*, 2014, **6**, 1922.
13 C. Liu, Z. Yu, D. Neff, A. Zhamu and B. Z. Jang, *Nano Lett.*, 2010, **10**, 4863.
14 X. Cao, Z. Yin and H. Zhang, *Energy Environ. Sci.*, 2014, **7**, 1850.
15 S. Bai and X. Shen, *RSC Adv.*, 2012, **2**, 64.
16 Y. Wang, Y. Wu, Y. Huang, F. Zhang, X. Yang, Y. Ma and Y. Chen, *J. Phys. Chem. C*, 2011, **115**, 23192.
17 W. Ai, W. Zhou, Z. Du, Y. Du, H. Zhang, X. Jia, L. Xie, M. Yi, T. Yu and W. Huang, *J. Mater. Chem.*, 2012, **22**, 23439.
18 Y. Xu, Z. Lin, X. Huang, Y. Wang, Y. Huang and X. Duan, *Adv. Mater.*, 2013, **25**, 5779.
19 W. Ai, Z. Z. Du, J. Q. Liu, F. Zhao, M. D. Yi, L. H. Xie, N. E. Shi, Y. W. Ma, Y. Qian, Q. L. Fan, T. Yu and W. Huang, *RSC Adv.*, 2012, **2**, 12204.
20 Y. H. So and J. P. Heeschen, *J. Org. Chem.*, 1997, **62**, 3552.
21 H. Jiang, C. Li, T. Sun and J. Ma, *Chem. Commun.*, 2012, **48**, 2606.
22 S. Stankovich, R. D. Piner, S. T. Nguyen and R. S. Ruoff, *Carbon*, 2006, **44**, 3342.
23 W. Ai, J. Q. Liu, Z. Z. Du, X. X. Liu, J. Z. Shang, M. D. Yi, L. H. Xie, J. J. Zhang, H. F. Lin, T. Yu and W. Huang, *RSC Adv.*, 2013, **3**, 45.

24 X. Zhang, Y. Huang, Y. Wang, Y. Ma, Z. Liu and Y. Chen, *Carbon*, 2009, **47**, 334.
25 J. Lim, T. A. Albright, B. R. Martin and O. S. Miljanic, *J. Org. Chem.*, 2011, **76**, 10207.
26 S. Song, Y. Xue, L. Feng, H. Elbatal, P. Wang, C. N. Moorefield, G. R. Newkome and L. Dai, *Angew. Chem., Int. Ed.*, 2014, **53**, 1415.
27 J. S. Lee, K. H. You and C. B. Park, *Adv. Mater.*, 2012, **24**, 1084.
28 G. Wang, X. Shen, B. Wang, J. Yao and J. Park, *Carbon*, 2009, **47**, 1359.
29 K. N. Kudin, B. Ozbas, H. C. Schniepp, R. K. Prud'homme, I. A. Aksay and R. Car, *Nano Lett.*, 2008, **8**, 36.
30 D. R. Dreyer, S. Park, C. W. Bielawski and R. S. Ruoff, *Chem. Soc. Rev.*, 2010, **39**, 228.
31 C. Gomez-Navarro, R. T. Weitz, A. M. Bittner, M. Scolari, A. Mews, M. Burghard and K. Kern, *Nano Lett.*, 2007, **7**, 3499.
32 V. Paul-Boncour, S. F. Parker, H. Hagemann, S. M. Filipek, R. Wierzbicki and M. Latroche, *Faraday Discuss.*, 2011, **151**, 307.
33 Z. Du, W. Ai, J. Zhao, L. Xie and W. Huang, *Sci. China: Technol. Sci.*, 2014, **57**, 244.
34 Y. Tao, H. Kanoh, L. Abrams and K. Kaneko, *Chem. Rev.*, 2006, **106**, 896.
35 D. W. Wang, F. Li, Z. S. Wu, W. Ren and H. M. Cheng, *Electrochem. Commun.*, 2009, **11**, 1729.
36 L. Sun, L. Wang, C. Tian, T. Tan, Y. Xie, K. Shi, M. Li and H. Fu, *RSC Adv.*, 2012, **2**, 4498.
37 Y. Yoon, K. Lee, C. Baik, H. Yoo, M. Min, Y. Park, S. M. Lee and H. Lee, *Adv. Mater.*, 2013, **25**, 4437.
38 L. Sun, C. Tian, Y. Fu, Y. Yang, J. Yin, L. Wang and H. Fu, *Chem.–Eur. J.*, 2014, **20**, 564.
39 L. L. Zhang, X. Zhao, M. D. Stoller, Y. Zhu, H. Ji, S. Murali, Y. Wu, S. Perales, B. Clevenger and R. S. Ruoff, *Nano Lett.*, 2012, **12**, 1806.
40 F. Zeng, Y. Kuang, G. Liu, R. Liu, Z. Huang, C. Fu and H. Zhou, *Nanoscale*, 2012, **4**, 3997.
41 J. Cao, Y. Wang, P. Xiao, Y. Chen, Y. Zhou, J. H. Ouyang and D. Jia, *Carbon*, 2013, **56**, 389.
42 W. Ai, L. Xie, Z. Du, Z. Zeng, J. Liu, H. Zhang, Y. Huang, W. Huang and T. Yu, *Sci. Rep.*, 2013, **3**, 2341.
43 Z. Du, W. Ai, L. Xie and W. Huang, *J. Mater. Chem. A*, 2014, **2**, 9164.
44 L. Sun, C. Tian, M. Li, X. Meng, L. Wang, R. Wang, J. Yin and H. Fu, *J. Mater. Chem. A*, 2013, **1**, 6462.